Characterization of Stiffness and Damping in Textured Sector Pad Micro Thrust Bearings Using Computational Fluid Dynamics

Christos I. Papadopoulos[1]
School of Naval Architecture
and Marine Engineering,
National Technical University of Athens,
15710 Zografos, Greece
e-mail: chpap@central.ntua.gr

Pantelis G. Nikolakopoulos
Machine Design Laboratory,
Department of Mechanical
Engineering and Aeronautics,
University of Patras,
26504 Patras, Greece
e-mail: pnikolak@mech.upatras.gr

Lambros Kaiktsis
School of Naval Architecture
and Marine Engineering,
National Technical University of Athens,
15710 Zografos, Greece
e-mail: kaiktsis@naval.ntua.gr

In the present paper, a study of stiffness and damping in sector-pad micro thrust bearings with artificial surface texturing is presented, based on computational fluid dynamics (CFD) simulations. The bearing pads are modeled as consecutive three-dimensional independent microchannels, each consisting of a smooth rotating wall (rotor) and a partially textured stationary wall (stator). CFD simulations are performed, consisting in the numerical solution of the Navier–Stokes equations for incompressible isothermal flow. The goal of the present study is to characterize the dynamic behavior of favorable designs, identified in previous optimization studies, comprising parallel and convergent thrust bearings with rectangular texture patterns. To this end, a translational degree of freedom (DOF) along the thrust direction and a rotational (tilting) DOF of the rotor are considered. By implementing appropriate small perturbations around the equilibrium (steady-state) position and processing the simulation results, the stiffness and damping coefficients of the bearing are obtained for each DOF. The computed dynamic coefficients of textured thrust bearings are compared to those of conventional (smooth slider) designs. It is found that the dependence of bearing stiffness and damping on geometrical parameters exhibits the same trends for both DOFs. Both stiffness and damping are found to increase with bearing width. In general, increasing the bearing convergence ratio results in increased bearing stiffness and decreased damping. Finally, the present results demonstrate that properly textured parallel sliders are characterized by an overall dynamic performance that is superior to that of smooth converging sliders.
[DOI: 10.1115/1.4007320]

Keywords: 3D micro thrust bearings, sector pad, stiffness, damping, CFD

Introduction

The performance of micro thrust and journal bearings is important for the overall performance and dynamic behavior of rotating microengines [1–3]. For micro thrust bearing applications, recent research has demonstrated that properly designed texture patterns may substantially increase bearing performance. Recent technological advances in surface treatment enable the introduction of such designs, with resolution accuracy in the micron scale [4]. The performance potential of texture patterns in improving bearing performance has been demonstrated in recent computational studies utilizing the Reynolds equation [5–9], as well as in recent CFD studies [9–12]. Lately, optimization studies of bearing texture patterns have been reported, aiming at an identification of proper texture geometry parameters, for optimal bearing performance [13–17]. The latter is commonly expressed by the two principal bearing performance indices, the load carrying capacity and the friction coefficient.

In addition to providing optimal static performance, bearing designs should also contribute to a proper dynamic performance, providing satisfactory stiffness and damping properties. The dynamic characteristics of untextured journal/thrust bearings have been the subject of several studies, including Refs. [18–25]. To the authors' knowledge, studies on the dynamic characteristics of textured thrust bearings have not yet been reported.

Thus, following the optimization study of 3D textured micro thrust bearings of Ref. [17], the present work aims at characterizing the dynamic properties of optimal 3D textured micro thrust bearings, using CFD. The properties considered here are the bearing stiffness and damping with respect to translational (i.e., in the thrust direction) and tilting motions; these properties are quantified by proper nondimensional indices.

The paper is organized as follows: The problem definition and computational approach are first presented, including model validation tests. Simulation results are then presented and discussed, and, finally, the main findings are summarized.

Problem Definition

Micro Thrust Bearing Geometry. In Fig. 1, the top views of three eight-pad thrust bearings are presented, with values of width-to-length ratio, B/L, defined for the pad midsector, equal to 0.5, 1.0, and 1.5. In the present study, the number of bearing pads N_p is maintained to $N_p = 8$. Consecutive pads are separated by

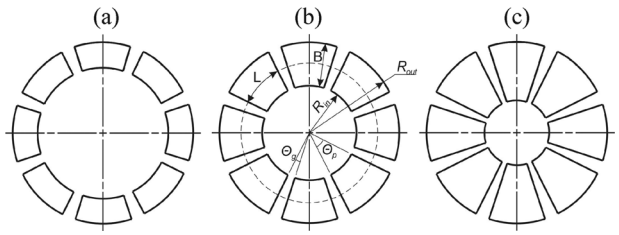

Fig. 1 Top view of eight-pad thrust bearings for (*a*) $B/L = 0.5$, (*b*) $B/L = 1.0$, (*c*) $B/L = 1.5$

[1]Corresponding author.

Contributed by International Gas Turbine Institute (IGTI) of ASME for publication in the JOURNAL OF ENGINEERING FOR GAS TURBINES AND POWER. Manuscript received June 15, 2012; final manuscript received July 18, 2012; published online September 20, 2012. Editor: Dilip R. Ballal.

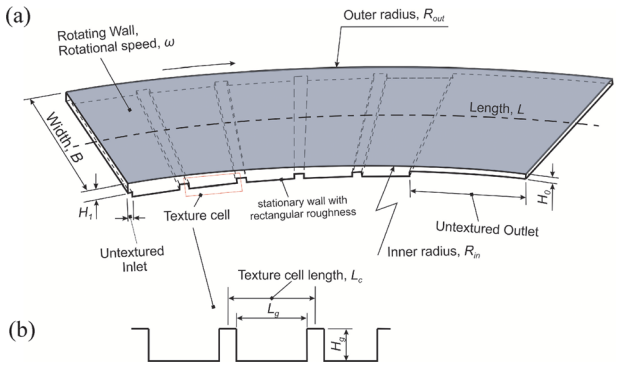

Fig. 2 (*a*) Geometry of the fluid domain of a textured thrust bearing pad, (*b*) texture geometry parameters, defined at the pad midsector

grooves; the area occupied by each pad or groove is determined by a corresponding angle Θ_p or Θ_g (see Fig. 1). These angles are controlled by the nondimensional parameters $\vartheta_p = \Theta_p/(\Theta_p + \Theta_g)$, $\vartheta_g = \Theta_g/(\Theta_p + \Theta_g)$. In the present work, Θ_p is taken equal to 0.8 (thus, $\Theta_g = 0.2$).

The geometry of a single micro thrust bearing pad with partial periodic rectangular texturing is presented in Fig. 2. The fluid convects towards the outlet and builds up pressure, which exerts forces on the bearing walls. Pressure buildup is due to the presence of rectangular grooves, extending in the spanwise (radial) direction over the bearing width and (possibly) also due to the converging geometry. Force equilibrium is attained by the presence of an external vertical load W on both walls. Energy is expended by the work done by the shear forces at the moving wall–fluid interface.

A three-dimensional parametric computer-aided design (CAD) model has been built, with geometry dimensions representative of microbearings. The bearing has a width of B in the radial direction. All other lengths are defined at the pad midsector. The bearing height changes from the pad inlet height H_1 to its value H_0 at the pad outlet. H_0 and H_1 are controlled by the value of the convergence ratio $k = (H_1 - H_0)/H_0$. Evidently, zero values of k account for parallel geometries, while positive values of k correspond to converging geometries. In the present study, the value of minimum film thickness $H_{\min}$ is assumed in all cases constant, equal to 0.05 mm. The length L of the pad is controlled by the nondimensional parameter $l = L/H_{\min}$; here l is equal to 100. The bearing width B is controlled by the ratio B/L.

Part of the stationary wall is textured with rectangular grooves (Fig. 2). For all cases, an untextured part (sill) at the inlet, of length equal to 1/100 of the total length, i.e., $l_{ui} = 0.01$, is considered. The untextured length at the pad outlet is controlled by the nondimensional parameter l_{uo}. The textured part exhibits N periodic texture cells. Each texture cell is defined by the cell length L_c, the groove length L_g, and the groove depth H_g (see Fig. 2(*b*)). These dimensional geometric parameters are controlled by the texture density $\rho_T = L_g/L_c$, and the relative groove depth $s = H_g/H_{\min}$.

Governing Equations and Assumptions. The flow is considered isothermal, and the minimum pressure value is assumed to be above the vapor pressure; thus, cavitation is not accounted for. The conservation equations for unsteady incompressible and isothermal flow, with zero gravitational and other external body forces, are:

- Mass conservation equation

$$\nabla \cdot \mathbf{V} = 0 \tag{1}$$

- Momentum equations

$$\frac{\partial \mathbf{V}}{\partial t} + \mathbf{V} \cdot \nabla \mathbf{V} = -\frac{1}{\rho}\nabla p + \frac{\mu}{\rho}\nabla^2 \mathbf{V} \tag{2}$$

where $\mathbf{V}$ is the velocity vector, p the static pressure, ρ the fluid density, and μ the dynamic viscosity.

Equations (1) and (2) are solved with a commercial CFD software, utilizing a finite volume approach. From dimensional analysis, it follows that, for given geometry, the flow dynamics depends on the Reynolds number Re, defined at the bearing midsection, in terms of the local moving wall velocity $U = \omega R_{\text{mean}}$ and the minimum film thickness $H_{\min}$ (ω is the rotor angular velocity and R_{mean} the radius at the pad midsector). Simulations are performed for $\text{Re} = 1$, a value representative of microbearing applications. In the present dimensional model, a value of $\text{Re} = 1$ corresponds to a velocity $U = 0.01785\,\text{ms}^{-1}$ at the pad midsector, and values of the fluid thermophysical properties equal to those of water at 25 °C (see Ref. [16]). Results are presented in nondimensional form.

Spatial Discretization, Boundary and Initial Conditions. Depending on flow symmetries of a particular case studied, either the full geometry (eight-pad for tilting disturbances) or one pad (for translational disturbances) is modeled (see Fig. 1). Typical 3D meshes generated consist of approximately 200,000 hexahedral finite volumes per bearing pad. During load variation, since the instantaneous channel height changes every time step, the grid is adapted accordingly; the adaptation maintains the total number of finite volumes. The corresponding finite volume size in the cross-flow direction of the slider is 0.04 $H_{\min}$–0.1 $H_{\min}$, with a minimum of 15 cells in the untextured region, along the cross-flow direction. The grid is denser in near-wall regions (see Ref. [16] for details on grid design). In the streamwise (circumferential) direction, the finite volume size is approximately 0.1 $H_{\min}$–0.2 $H_{\min}$ at the midsector of the pads. In the spanwise (radial) direction, the discretization utilizes a typical finite volume size of approximately 1–2 $H_{\min}$. Spatial resolution tests have been performed by generating meshes with numbers of finite volumes both lower and substantially higher than the typical meshes used. The relative differences in the flow integral quantities (load capacity and dynamic coefficients) between typical and very fine meshes were in all cases on the order of 1%.

The bearing walls are considered impermeable. The bottom (textured) wall is stationary. The upper wall is assumed to be moving at a constant angular velocity ω, with a local circumferential velocity $U = \omega r$ at the pad midsector, r being the local radius. No-slip conditions are assumed at both walls.

The inlet and outlet surfaces of a bearing pad (see Figs. 1 and 2) are considered openings: The pressure is assumed constant, with the same value $p = 0$ prescribed at both boundaries, while a Neumann boundary condition is assumed for the velocity. At the bearing sides $r = R_{in}, R_{out}$, an outflow condition is prescribed, i.e., in addition to the above assumptions, no inflow to the computational domain is allowed. This boundary condition corresponds to thrust bearings with direct injection of lubricating oil in the grooves between consecutive pads. For fully flooded bearings, an opening type of boundary condition (permitting both outflow and inflow) would be appropriate. Nonetheless, parametric studies with both types of boundary conditions (carried out for optimal textured bearings of $B/L = 0.5$—for which the effect of boundary condition is expected to be more pronounced) demonstrate only a slight overestimation in load carrying capacity at low convergence ratio values for flooded bearings; this overestimation practically vanishes for $k \geq 0.4$.

All simulations were initialized from zero velocity and pressure fields. For the present Reynolds number $\text{Re} = 1$, the governing equations were integrated for a total time of 60 dimensionless time units ($t^* = tU/H_{\min}$), resulting in all cases in steady state. Convergence to steady state was verified by monitoring the computed velocity and pressure at a number of representative points within the flow domain.

The average vertical force exerted to a rotor pad area is calculated by integrating the instantaneous pressure p over the rotor surface:

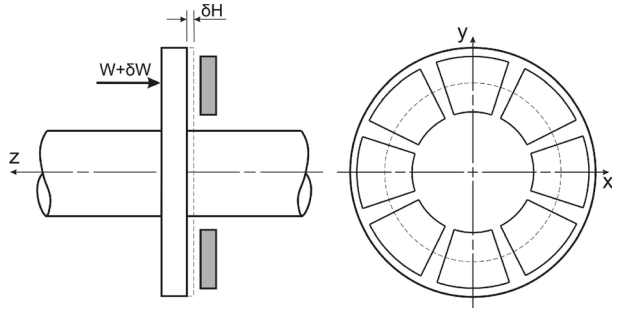

Fig. 3 Sketch of translational motion of the rotor of a sector pad thrust bearing

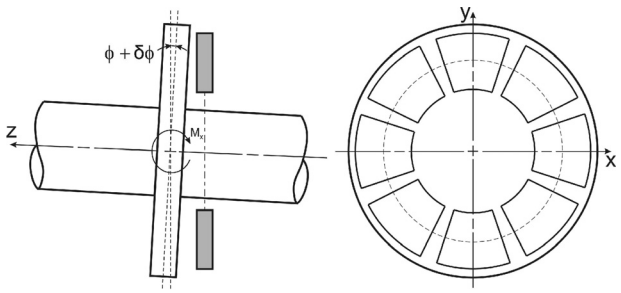

Fig. 4 Sketch of tilting motion of the rotor of a sector pad thrust bearing

$$F_p = \frac{1}{N_p}\int_A p\,dA = W \tag{3}$$

where A is the total area of bearing pads.

The average moment exerted to a rotor pad can be readily calculated:

$$M_x = \frac{1}{N_p} M_{x,tot} \tag{4}$$

where $M_{x,tot}$ is the total moment of the bearing with respect to the x-axis.

Stiffness and Damping Coefficients. The stiffness and damping coefficients of sector pad thrust bearings are computed for two types of rotor motion, namely a translational motion along the thrust direction (Fig. 3) and a tilting motion with reference to a principal axis of symmetry of the rotor (Fig. 4). The CFD simulations implement the perturbation pattern presented in Fig. 5. Here, three consecutive stages are considered:

(a) Initial stage: The rotor is set to rotation at a constant angular velocity, exhibiting no translational or tilting motion. Pressure builds up and steady-state conditions are reached.
(b) Perturbation stage: A (gradual) small perturbation to the film thickness around the equilibrium is imposed, corresponding to either a translation or a rotation of the bearing rotor. The instantaneous values of load carrying capacity or moment, and the corresponding translational or tilting velocities of the rotor are recorded. Here, a mesh deformation technique is utilized to account for the changing fluid film volume. By processing the simulation results, the damping coefficient is calculated.
(c) Relaxation stage: Steady-state conditions are reached, corresponding to a new equilibrium position (final state of the modified fluid film geometry). The stiffness coefficient is calculated.

In the present study, a total perturbation in film thickness of $0.01H_{\min}$ is used to calculate the translational stiffness and instantaneous damping coefficients, as follow:

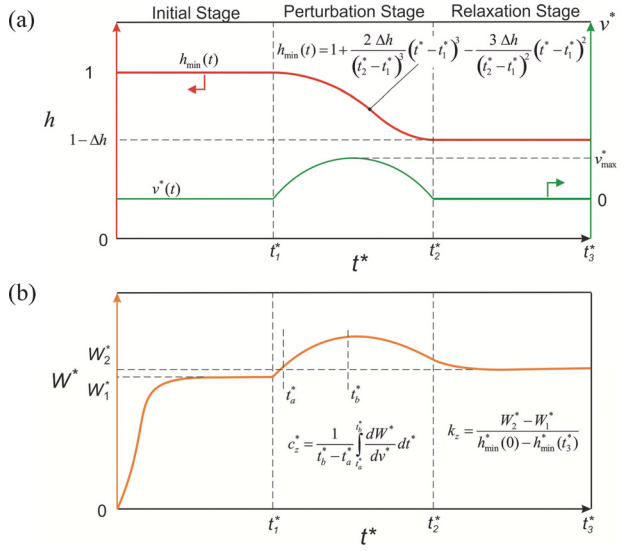

Fig. 5 Illustration of computation procedure of translational stiffness and average damping coefficient of thrust bearings: (*a*) imposed temporal variation of film thickness and corresponding rotor cross-flow (squeeze) velocity, and (*b*) resulting variation of load carrying capacity

- Translational stiffness coefficient

$$k_z \simeq \frac{\Delta W}{\Delta H} \tag{5}$$

- Nondimensional translational stiffness coefficient

$$k_z^* = k_z \frac{H_{\min}^3}{BL^2 U\mu} \tag{6}$$

- Instantaneous translational damping coefficient

$$c_{z,inst} \simeq \frac{\delta W}{\delta v} \tag{7}$$

where v is the instantaneous translational (squeeze) velocity.

- Nondimensional instantaneous translational damping coefficient

$$c_{z,inst}^* = c_{z,inst} \frac{U}{L} \frac{H_{\min}^3}{BL^2 U\mu} \tag{8}$$

In the case of tilting motions of the rotor, an appropriate perturbation angle is used, which corresponds to maximum change in film thickness of $0.001\,H_{\min}$ in a pad midsection. The rotational stiffness and instantaneous damping coefficients of the bearing are calculated as follow:

- Rotational stiffness coefficient

$$k_\phi \simeq \frac{\Delta M_x}{\Delta \phi} \tag{9}$$

where ϕ is the tilting angle (see Fig. 4)

- Nondimensional rotational stiffness coefficient

$$k_\phi^* = k_\phi \frac{H_{\min}^3}{B^2 L^3 U\mu} \tag{10}$$

- Instantaneous rotational damping coefficient

$$c_{\phi,inst} \simeq \frac{\delta M_x}{\delta \dot{\phi}} \tag{11}$$

• Nondimensional instantaneous rotational damping coefficient

$$c^*_{\phi,inst} = c_{\phi,inst}\frac{U}{L}\frac{H^3_{\min}}{B^2L^3U\mu} \tag{12}$$

The average value of the (translational or rotational) damping coefficient over a time interval (t_a, t_b) can be readily calculated:

$$c^* = \frac{1}{t^*_b - t^*_a}\int_{t^*_a}^{t^*_b} c^*_{inst}(t^*)dt^* \tag{13}$$

The outcome of the simulation design proposed here, consisting of an initial (convergence to steady state), a perturbation, and a relaxation stage, is equivalent to that of two static and one transient analyses, leading to the simultaneous calculation of the stiffness and the average damping coefficients of the bearing. The duration of the different stages of each simulation is controlled by the nondimensional times t^*_1, t^*_2, t^*_3, t^*_a, and t^*_b (see Fig. 5). For selecting these nondimensional time parameters, the following were considered:

(a) Selection of parameters t^*_1 and t^*_3:
Confirming convergence to steady state (prior to and after implementing the perturbation pattern) is important for accurately calculating the stiffness coefficient. To this end, based on characteristic time estimates and initial test runs, the values of $t^*_1 = 60$ and $t^*_3 = 100$ have been utilized.

(b) Selection of parameter t^*_2:
The duration of the perturbation stage $(t^*_2 - t^*_1)$ has been 10 nondimensional time units in all simulations reported subsequently; for translational rotor motions, this value corresponds to an average nondimensional squeeze velocity $v^* = \Delta z^*/(t^*_2 - t^*_1) = 0.001$. It is noted that the duration of the perturbation stage (equivalently: the squeeze velocity) affects the computed values of the (average) damping coefficient: Fig. 6 presents the nondimensional damping coefficient as a function of the nondimensional mean translational (squeeze) velocity, for optimal textured parallel thrust bearings of different B/L values. The damping coefficient is shown to be a mildly decreasing function of squeeze velocity for values of v^* lower than 0.001. The decrease becomes more pronounced for values of v^* larger than 0.001, especially for bearings with large B/L.

(c) Selection of parameters t^*_a and t^*_b:
The average value of damping coefficient has been calculated in the interval (t^*_a, t^*_b). For t^*_a, a value of 61 nondimensional time units has been selected, to neglect (nonphysical) load capacity fluctuations at the start of the perturbation stage $(t^* = t^*_1 = 60)$. A value of 64 nondimensional time units has been selected for t^*_b, to neglect values of the instantaneous damping coefficient in the regime where the velocity derivative is nearly zero (around $t^* = 65$), for which the numerical calculation of the instantaneous damping coefficient is problematic.

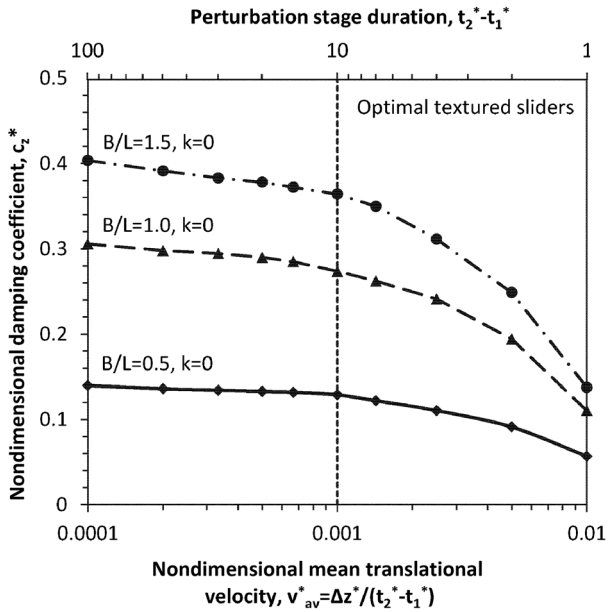

Fig. 6 Nondimensional average damping coefficient as a function of nondimensional mean translational (squeeze) velocity for optimal textured parallel thrust bearings with different values of *B/L* ratio. The geometry details are based on the optimization study of Ref. [17].

Validation of CFD Results. The present CFD model was validated by comparing computational results against published literature data for two problems relevant to the present study. First, a similar flow problem in a 2D converging textured bearing was solved, and the results compared against the CFD results of Ref. [10]. This problem consists of a textured slider bearing exhibiting three rectangular grooves, as shown in Fig. 7(*a*) (inset

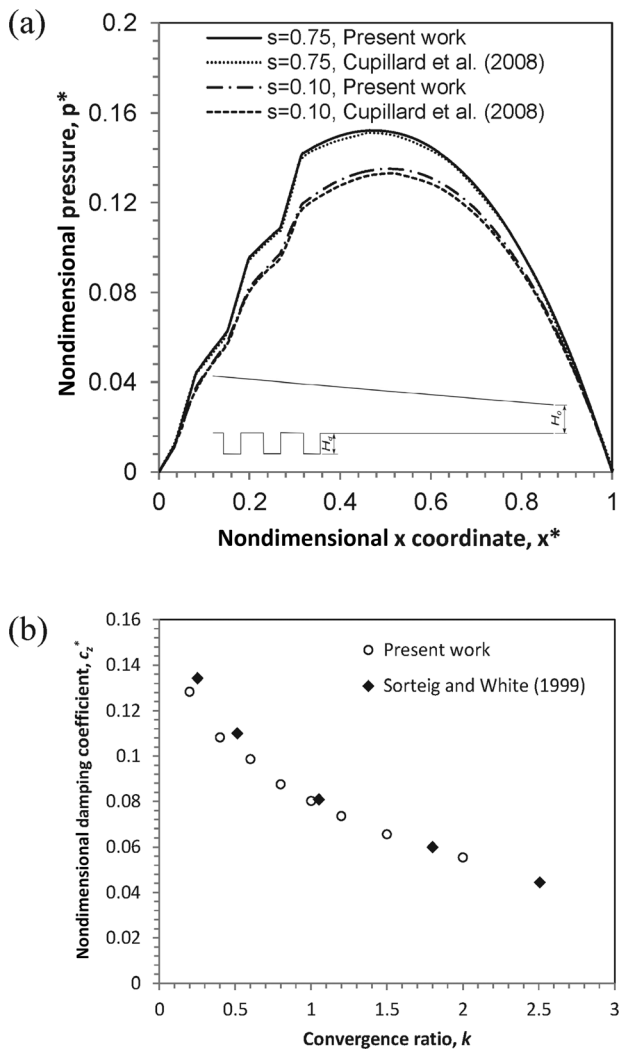

Fig. 7 Validation of present CFD results against literature data: (*a*) computed nondimensional pressure distribution versus nondimensional streamwise coordinate for a converging microbearing with texturing; (*b*) computed nondimensional average translational damping coefficient versus convergence ratio of rectangular tapered-land sliders with *B/L* = 0.5

Table 1 Correlations for parameters of optimal texture geometry, as reported in Ref. [17] ($N = 5$, $\rho_T = 0.83$)

B/L ratio	Untextured outlet length l_{uo}	Relative groove depth s	Optimal convergence ratio k_{opt}
0.5	$l_{uo} = 0.132\,k + 0.532$	$s = 0.006\,k + 0.372$	1.3
1.0	$l_{uo} = 0.109\,k + 0.447$	$s = -0.095\,k + 0.412$	1.1
1.5	$l_{uo} = 0.044\,k + 0.431$	$s = -0.277\,k + 0.492$	0.99

The reported value of k_{opt} corresponds to the global maximum in load carrying capacity

sketch). The bearing height at outlet H_0 is 0.03 mm; the bearing nondimensional length is $l = 200$. The length of each groove L_g is 0.3 mm; the texture density ρ_T is equal to 0.429, whereas two different values of $s = H_g/H_{\min}$ are considered, namely 0.75 and 0.1. The Reynolds number is equal to 1. Figure 7(*a*) presents the distribution of computed pressure along the moving wall, as well as the results of Ref. [10], illustrating a very good agreement.

As a second test, calculations were performed for 3D smooth tapered-land sliders of $B/L = 0.5$, and various convergence ratio values, and processed for the nondimensional translational damping coefficient ($N_p = 10$, $\mathrm{Re} = 1$). In Fig. 7(*b*), the results are compared against the published data of Ref. [23] (Reynolds equation), illustrating a very good agreement.

Optimal Geometry Parameters of Reference Textured Bearings. In the present study, the textured bearings considered are characterized by a maximum (optimal) nondimensional load carrying capacity $W^* = W/(\mu UB)(H_{\min}/L)^2$; their texture geometry is the outcome of the optimization studies reported in Ref. [17], which have utilized 3D rectangular channel geometries. The results in Ref. [17], corresponding to constant values of groove number and groove density ($N = 5$, $\rho_T = 0.83$), demonstrate that, for a given value of B/L, the optimal texture geometries, as defined by the untextured outlet length l_{uo} and the relative groove depth s, can be approximated by linear functions of convergence ratio k. These functions, along with the value of k_{opt}, corresponding to maximum load carrying capacity, are presented in Table 1.

Computational Results

Effect of Slider Model on Load Carrying Capacity. The present study utilizes the optimal texture patterns obtained in Ref. [17] for rectangular sliders. As the present work involves the study of dynamic coefficients associated with tilt motions of the rotor, sector-pad (nonrectangular) thrust bearing geometries must be utilized. Therefore, an initial assessment quantifying the discrepancy in the major performance index (load carrying capacity) between rectangular and sector pad sliders is necessary. Here, eight-pad sector thrust bearings are considered. Computed pressure distributions are processed to yield the instantaneous load carrying capacity. A representative pressure distribution is illustrated in Fig. 8, corresponding to the steady (unperturbed) state of an optimal textured eight-pad parallel bearing with $B/L = 1.0$.

Figure 9 presents simulation results in terms of load carrying capacity versus convergence ratio, for three representative values of B/L, for smooth and optimal textured sliders. For smooth sliders, calculations with a rectangular and a sector-pad slider model are practically equivalent; rectangular sliders exhibit slightly higher load carrying capacity values, with the maximum deviation being about 2% at small values of convergence ratio (Fig. 9(*a*)). The comparison of results remains good for the case of textured bearings (Fig. 9(*b*)). Specifically, rectangular textured sliders of $B/L = 0.5$ are characterized by slightly increased values of W^*, compared to those of sector pad sliders, with a maximum deviation of approximately 3.5% at small values of convergence

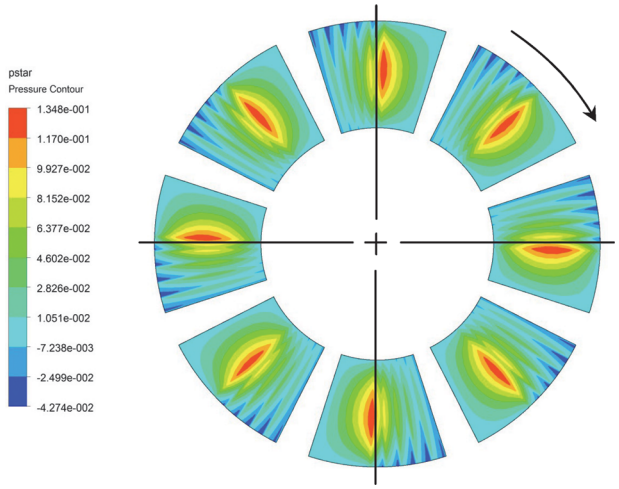

Fig. 8 Color-coded contours of steady-state nondimensional pressure on the rotor surface of an optimal textured eight-pad parallel thrust bearing with $B/L = 1.0$ ($l_{uo} = 0.447$, $s = 0.412$)

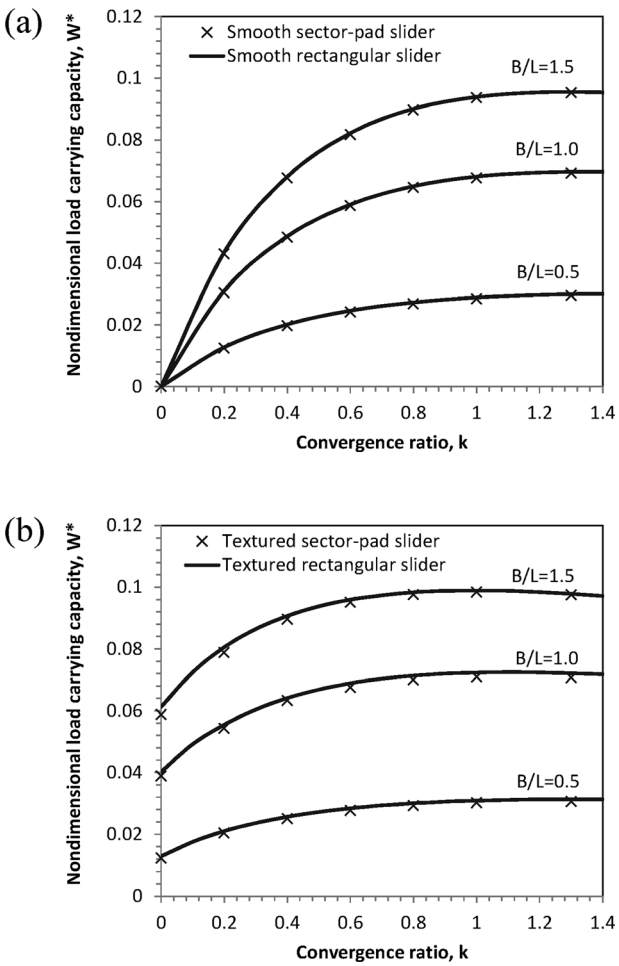

Fig. 9 Nondimensional load carrying capacity W^* versus convergence ratio k for different B/L values, for sector-pad and rectangular sliders: (*a*) smooth sliders, (*b*) optimal textured sliders

ratio. This overestimation decreases at increasing B/L and k, reaching approximately 0.5% for $B/L = 1.5$ and $k = 1.3$. These results demonstrate that rectangular slider models can be used to accurately predict load carrying capacity over a wide range of convergence and width-to-length ratios, both for smooth and

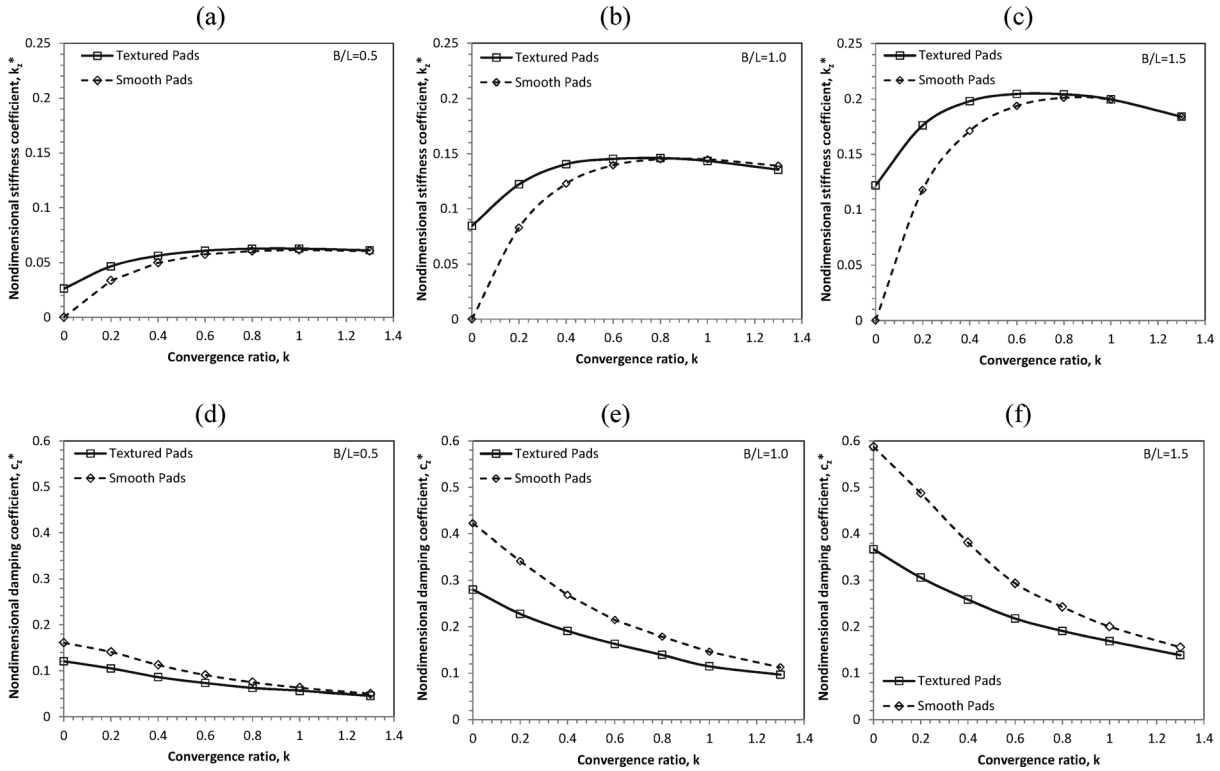

Fig. 10 Nondimensional translational stiffness and average damping coefficients k_z^* and c_z^* versus convergence ratio, k, for smooth and textured sector-pad sliders: (*a*,*d*) $B/L = 0.5$, (*b*,*e*) $B/L = 1.0$, (*c*,*f*) $B/L = 1.5$

optimal textured sliders, i.e., the results of Ref. [17] are also relevant for sector-pad geometries.

Dynamic Coefficients of Sector-Pad Thrust Bearings. Following the methodology outlined in the section Stiffness and Damping Conefficients, the dynamic coefficients of smooth and textured sector-pad thrust bearings are computed, for a wide range of B/L and convergence ratio values. The cases considered correspond to two types of rotor motion: (a) a translational (squeeze) motion along the thrust direction, and (b) a tilting motion with reference to a principal symmetry axis of the rotor (x-axis or y-axis of Fig. 3).

Figures 10(*a*)–10(*c*) present the computed nondimensional translational stiffness coefficient versus convergence ratio, for the three B/L values of the present study; results for both smooth and optimal textured sliders are included. As shown in Figs. 10(*a*)–10(*c*), there is a clear increase in the overall level of stiffness coefficient values with the increase of B/L. Further, bearing stiffness is an increasing function of convergence ratio, k, up to a certain value of k, which is found to be a decreasing function of B/L.

Figures 10(*a*)–10(*c*) also demonstrate that textured bearings provide a substantial improvement in stiffness coefficient over smooth bearings for a wide range of convergence ratios; this improvement is maximal in the limit of parallel bearings and decreases at increasing values of k. This finding may be important in terms of bearing stability for applications involving operation in a broad range of thrust loads. In particular, considering a converging fixed-pad bearing operating at a nominal load, it is realized that a decrease in thrust load will result in a corresponding decrease of the effective instantaneous convergence ratio, due to the associated increase of fluid film thickness. For smooth sliders, this leads to a substantial decrease in stiffness coefficient (Figs. 10(*a*)–10(*c*)), which may in turn give rise to unstable bearing performance. In contrast, for optimal textured sliders, the presence of substantial levels of stiffness coefficient, even for parallel sliders, reduces the possibility of unstable behavior for the entire range of convergence ratios.

Figures 10(*d*)–10(*f*) present the computed values of nondimensional translational damping coefficient as a function of convergence ratio for the three B/L values of the present study. Figures 10(*d*)–10(*f*) demonstrate a clear increase in the values of damping coefficient at increasing B/L. Further, the damping coefficient decreases monotonically with k. Finally, textured sliders are characterized by decreased levels of damping coefficient, in comparison to those of smooth sliders, with the discrepancies increasing at increasing B/L and decreasing k. Nonetheless, in the limit of parallel sliders, textured sliders may be characterized by damping coefficients higher than those of high convergence ratio smooth sliders. Thus, considering the previously discussed advantages of parallel textured sliders in terms of stiffness performance, it appears that they can be an attractive alternative to smooth converging bearings, providing improved dynamic performance.

Figure 11 presents the computed nondimensional rotational stiffness and damping coefficients versus convergence ratio for the three B/L values considered here. By comparing with Fig. 10, it is realized that the computed results exhibit the same qualitative dependence on k and B/L for both the translational and the tilting motions.

Next, the sensitivity of the translational dynamic coefficients with respect to the principal texture design variables (relative groove depth s and nondimensional untextured outlet length l_{uo}) is investigated. Here, the case of $B/L = 0.5$ is considered for two representative values of convergence ratio, namely $k = 0$ (parallel sliders, Figs. 12(*a*)–12(*c*) and 13(*a*)–13(*c*)) and $k = k_{opt} = 1.3$ (Figs. 12(*d*)–12(*f*) and 13(*d*)–13(*f*)); for completeness, a corresponding curve for W^* is also included. In particular, Figs. 12(*a*)–12(*f*) present the dependence of W^*, k_z^*, c_z^* on s. It is demonstrated that the optimal (in terms of W^*) s-range of sector-pad bearings is also characterized by high k_z^* values, which suggests a clear relationship between load capacity and bearing stiffness. On the other hand, the damping coefficient c_z^* exhibits a monotonic decrease at increasing values of groove depth. The results of Fig. 13 demonstrate that, in varying l_{uo}, k_z^* is maximized in the range of optimal l_{uo} (i.e., corresponding to maximum W^*), while c_z^* increases monotonically with l_{uo}. Figures 12 and 13 show

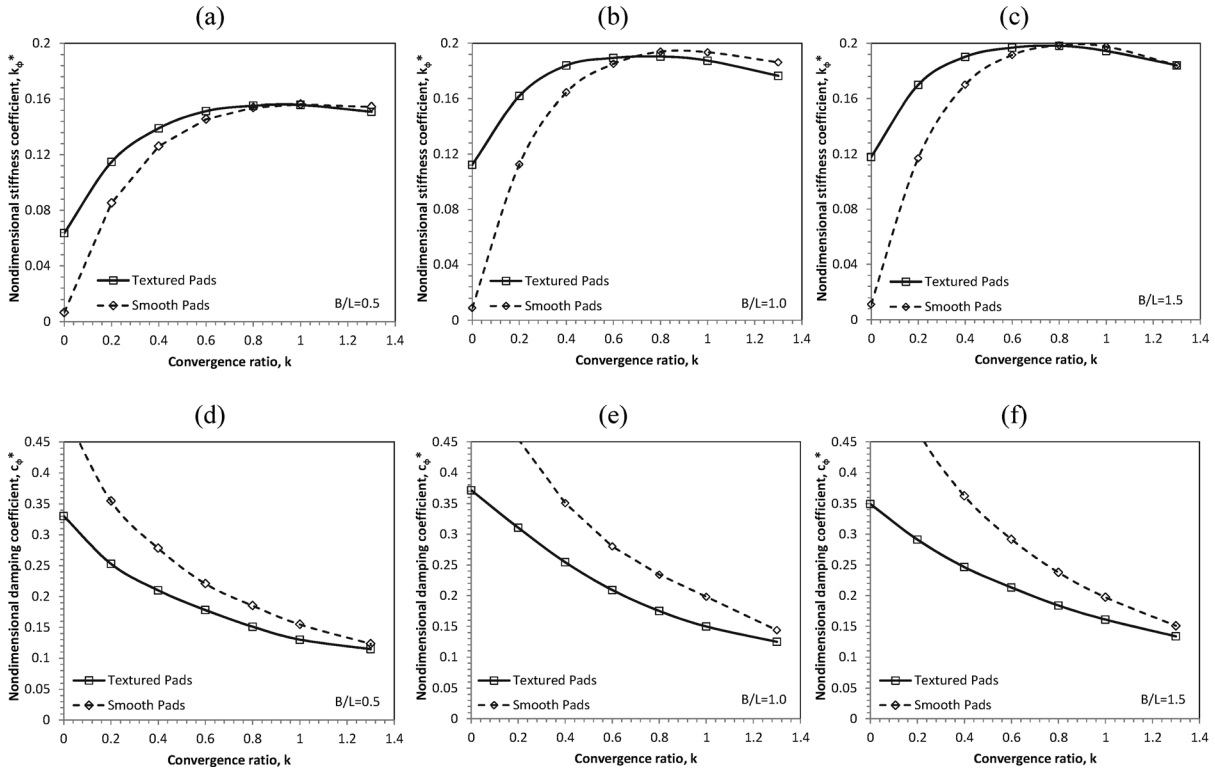

Fig. 11 Nondimensional rotational stiffness and average damping coefficients k_ϕ^* and c_ϕ^* versus convergence ratio, k, for smooth and textured sector-pad sliders: (a,d) $B/L = 0.5$, (b,e) $B/L = 1.0$, (c,f) $B/L = 1.5$

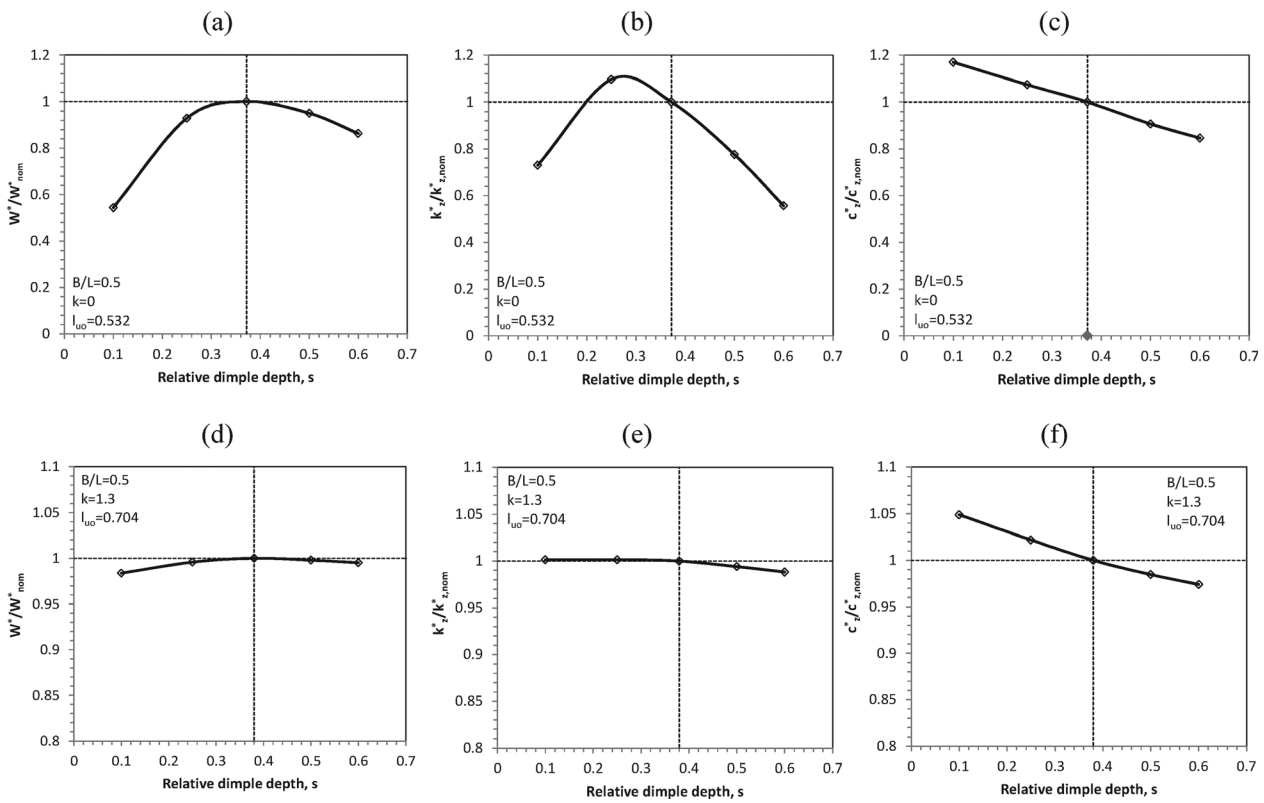

Fig. 12 Parallel textured bearings with $B/L = 0.5$. Variation of normalized: (a,d) nondimensional load carrying capacity, (b,e) nondimensional translational stiffness coefficient, and (c,f) nondimensional average translational damping coefficient, versus relative groove depth, for parallel (a–c) and converging with $k = k_{opt} = 1.3$ (d–f) textured sliders. The values of untextured outlet lengths l_{uo} are kept constant at their optimal values.

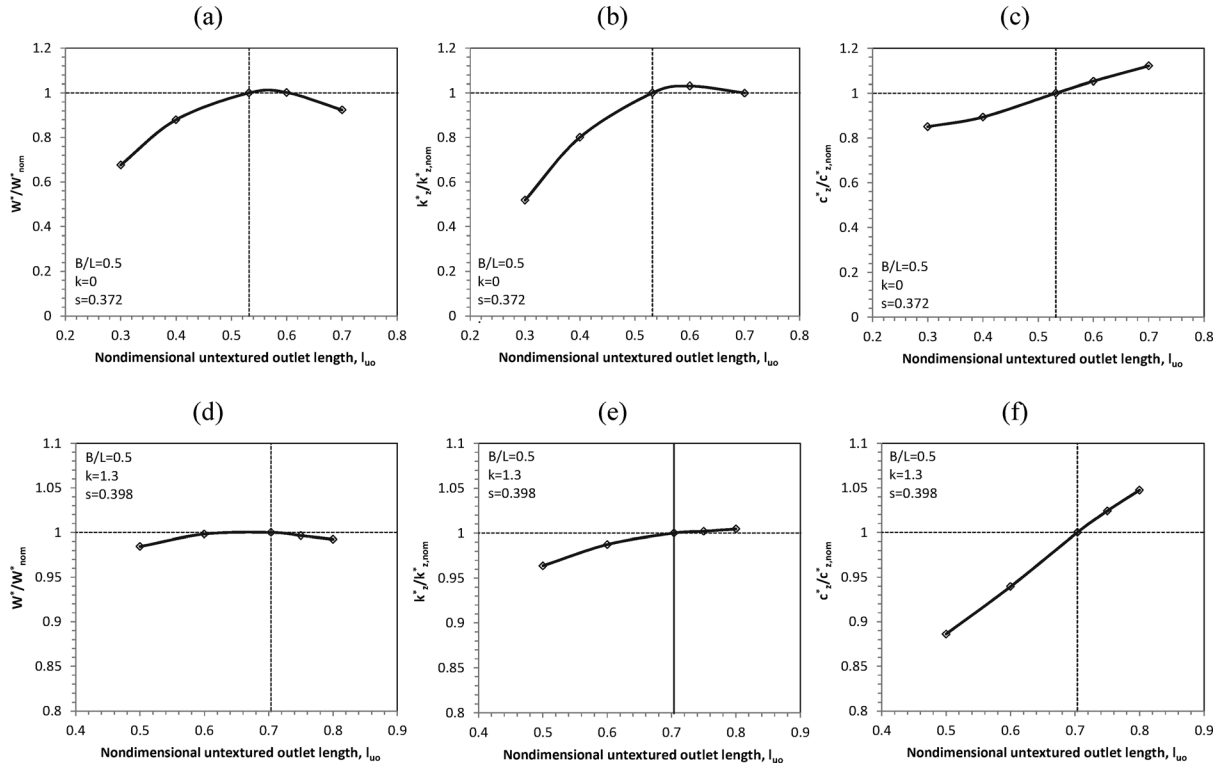

Fig. 13 Parallel textured bearings with *B/L* = 0.5. Variation of normalized: (*a*,*d*) nondimensional load carrying capacity, (*b*,*e*) nondimensional translational stiffness coefficient, and (*c*,*f*) nondimensional translational damping coefficient, versus untextured outlet length, for parallel (*a*–*c*) and converging with $k = k_{opt} = 1.3$ (*d*–*f*) textured sliders. The values of relative groove depths *s* are kept constant at their optimal values.

that converging sliders with $k = k_{opt} = 1.3$ demonstrate the same qualitative dependence of indices $\bar{W}^*$, k_z^*, c_z^* on the principal texture design variables (s, l_{uo}) as parallel sliders, however, with a decreased sensitivity to the variation of s, l_{uo}.

Conclusions

In the present work, a CFD study of stiffness and damping in three-dimensional sector-pad micro thrust bearings with artificial surface texturing has been presented. Here, the bearing texture parameters were based on the results of the optimization study reported in Ref. [17]. Two uncoupled degrees of freedom, corresponding to a translational and a tilting motion of the rotor, have been considered. For the computation of the corresponding stiffness and damping coefficients, integrated CFD simulations, consisting of an initial, a perturbation, and a relaxation stage, have been designed. Nondimensional stiffness and damping coefficients have been computed for smooth and optimal textured micro thrust bearings over a wide range of B/L and convergence ratios. The dependence of bearing stiffness and damping on geometrical parameters has been found to be qualitatively the same for both translation and tilting. The trends identified can be summarized as follows:

- The stiffness of both textured and smooth bearings increases with the bearing width-to-length ratio B/L. Up to a certain level, an increase in the bearing convergence ratio k results in increased bearing stiffness.
- Optimal textured bearings provide improved stiffness over smooth bearings for a wide range of k values.
- Bearing damping increases with B/L, while it decreases monotonically with k.
- In optimal textured sliders, damping levels are lower than those of smooth sliders.
- Parallel textured sliders are characterized by an overall dynamic behavior that is superior to that of smooth converging bearings.

An important outcome of the present work regards the significance of parallel textured sliders for thrust bearing applications. As demonstrated here, parallel sliders exhibit good dynamic properties, which; in addition, are load independent; further, their load capacity, although lower than that of optimal converging (smooth or textured) sliders, is still satisfactory (see Ref. [17]). Finally, parallel textured sliders are less sensitive to load variation in terms of load carrying capacity, while they are easier to manufacture. Overall, parallel textured sliders appear to be an efficient and cost-effective candidate for micromachine applications.

Based on the total development and computational results presented in Ref. [17] and in the present paper, an integrated CFD-based tool for the design and optimization of micro thrust bearings, in terms of both static and dynamic performance, is available. The results in Ref. [17], accompanied by those of the present study, can be utilized for dimensioning actual bearings for an overall (static and dynamic) optimized performance. Finally, the present results can be utilized in future computational studies addressing the issues of stability and frequency response of textured micro thrust bearings.

Acknowledgment

This work has been partially supported by the EU project MARINELIVE, Grant No. 264057. This support is gratefully acknowledged.

Nomenclature

Micro Thrust Bearing Geometry Variables (Figs. 1 and 2(*a*))

A = total area of bearing pads (m^2)
B = slider width (m)
B/L = slider width-to-length ratio

H = film thickness (m)
h = nondimensional film thickness: $h = H/H_{\min}$
H_0, H_1 = outlet, inlet height (m)
$H_{\min}$ = minimum film thickness (m): $H_{\min} = \min(H_0, H_1)$
k = convergence ratio: $k = (H_1 - H_0)/H_0$
L = pad length at pad midsector (m)
l = nondimensional slider length: $l = L/H_{\min}$
L_{ui} = untextured inlet length (m)
l_{ui} = nondimensional untextured inlet length: $l_{ui} = L_{ui}/L$
L_{uo} = untextured outlet length (m)
l_{uo} = nondimensional untextured outlet length: $l_{uo} = L_{uo}/L$
N_p = number of pads
r = radial coordinate (m)
R_{in} = inner sector pad radius (m)
R_{mean} = radius at pad midsector (m): $R_{\text{mean}} = (R_{in} + R_{out})/2$
R_{out} = outer sector pad radius (m)
Θ_g = groove angle (rad)
Θ_p = pad angle (rad)
ϑ_g = nondimensional groove angle: $\vartheta_g = \Theta_g/(\Theta_p + \Theta_g)$
ϑ_p = nondimensional pad angle: $\vartheta_p = \Theta_p/(\Theta_p + \Theta_g)$

Texture Geometry Variables (Fig. 2(*b*))

H_g = groove depth (m)
L_c = texture cell length (m): $L_c = L(1 - l_{ui} - l_{uo})/(N + \rho_T - 1)$
L_g = groove length (m)
N = number of grooves per bearing pad
s = relative texture depth: $s = H_g/H_{\min}$
ρ_T = texture density: $\rho_T = L_g/L_c$

Physics Variables

c_z = average translational damping coefficient (N s/m)
$c_{z,inst}$ = instantaneous translational damping coefficient (N s/m)
c_z^* = nondimensional average translational damping coefficient: $c_z^* = c_z H_{\min}^3/(BL^2U\mu)$
c_ϕ = average rotational damping coefficient (N m s/rad)
$c_{\phi,inst}$ = instantaneous rotational damping coefficient (N m s/rad)
c_ϕ^* = nondimensional average rotational damping coefficient: $c_\phi^* = c_\phi H_{\min}^3(U/L)/(B^2L^3U\mu)$
F_p = vertical pressure force (N)
k_z = translational stiffness coefficient (N/m)
k_z^* = nondimensional translational stiffness coefficient: $k_z^* = k_z H_{\min}^3/(BL^2U\mu)$
k_ϕ = rotational stiffness coefficient (N m/rad)
k_ϕ^* = nondimensional rotational stiffness coefficient: $k_\phi^* = k_\phi H_{\min}^3/(B^2L^3U\mu)$
M_x = average moment per bearing pad (N m)
p = pressure (Pa)
p^* = nondimensional pressure: $p^* = (p/\rho U^2)\text{Re}(H_{\min}/L)$
Re = Reynolds number: $\text{Re} = \rho U H_{\min}/\mu$
t = simulation time (s)
t^* = nondimensional simulation time: $t^* = tU/H_{\min}$
U = velocity at pad midsector (m s−1): $U = \omega R_{\text{mean}}$
$\mathbf{V}$ = fluid velocity vector
v = squeeze velocity component (m s^{-1})
W = average value of external bearing force per bearing pad (load carrying capacity) (N)
W^* = nondimensional load carrying capacity: $W^* = (W/\mu UB)(H_{\min}/L)^2$
μ = fluid dynamic viscosity (Pa s)
ρ = fluid density (kg m^{-3})
τ = shear stress (Pa)
ω = rotor angular velocity (rad/s): $\omega = U/R_{\text{mean}}$

References

[1] Shan, X. C., Zhang, Q. D., Sun, Y. F., and Maeda, R., 2007, "Studies on a Micro Turbine Device With Both Journal- and Thrust-Air Bearings," Microsystem Tech., **13**(11), pp. 1501–1508.
[2] Nakano, S., Kishibe, T., Inoue, T., and Shiraiwa H., 2009, "An Advanced Microturbine System With Water-Lubricated Bearings," Int. J. Rotating Mach., **2009**, pp. 1–12.
[3] Peirs, J., Reynaerts, D., and Verplaetsen, F., 2003, "Development of an Axial Microturbine for a Portable Gas Turbine Generator," J. Micromech. Microeng., **13**, (4), pp. 190–195.
[4] Hongyi, Y., Ratchev, S., Turitto, M., and Segal, J., 2009, "Rapid Manufacturing of Non-Assembly Complex Micro-Devices by Microsterolithography," Tsinghua Sci. Tech., **14**(S1), pp. 164–167.
[5] Etsion, I., Halperin, G., Brizmer, V., and Kligerman, Y., 2004, "Experimental Investigation of Laser Surface Textured Parallel Thrust Bearings," Tribol. Lett., **17**(2), pp. 295–300.
[6] Ozalp, A. A., and Umur, H., 2006, "Optimum Surface Profile Design and Performance Evaluation of Inclined Slider Bearings," Curr. Sci., **90**(11), pp. 1480–1491, available at: http://cs-test.ias.ac.in/cs/Downloads/article_40101.pdf.
[7] Pascovici, M. D., Cicone, T., Fillon, M., and Dobrica, M. B., 2009, "Analytical Investigation of a Partially Textured Parallel Slider," Pro. I. Mech. Eng. J-J.Eng. Tribol., **223**(2), pp. 151–158.
[8] Buscaglia, G. C., Ciuperca, I., and Jai, M., 2005, "The Effect of Periodic Textures on the Static Characteristics of Thrust Bearings," ASME J. Tribol., **127**(4), pp. 899–902.
[9] Dobrica, M. B., and Fillon, M., 2009, "About the Validity of Reynolds Equation and Inertia Effects in Textured Sliders of Infinite Width," Pro. I. Mech. Eng. J-J.Eng. Tribol., **223**(1), pp. 69–78.
[10] Cupillard, S., Cervantes, M. J., and Glavatskih, S., 2008, "Pressure Buildup Mechanism in a Textured Inlet of a Hydrodynamic Contact," ASME J. Tribol., **130**(2), pp. 1–10.
[11] Arghir, M., Roucou, N., Helene, M., and Frene, J., 2003, "Theoretical Analysis of the Incompressible Laminar Flow in a Macro-Roughness Cell," ASME J. Tribol., **125**(2), pp. 309–318.
[12] Han, J., Fang, L., Sun, J., and Ge S., 2010, "Hydrodynamic Lubrication of Microdimple Textured Surface Using Three-Dimensional CFD," Tribol. Trans., **53**(6), pp. 860–870.
[13] Van Marian, V. G., Kilian, M., and Scholz, W., 2007, "Theoretical and Experimental Analysis of a Partially Textured Thrust Bearing With Square Dimples," Pro. I. Mech. Eng. J-J.Eng. Tribol., **221**(7), pp. 771–778.
[14] Ostayen, R. A. J., Van Beek, A., and Munnig-Schmidt, R. H., 2007, "Film Height Optimization of Hydrodynamic Slider Bearings," Proceedings of the Society of Tribologists and Lubrication Engineers/American Society of Mechanical Engineers (STLE/ASME) 2007 International Joint Tribology Conference, San Diego, CA, October 22–24, ASME Paper No. IJTC2007-44191, pp. 237–239.
[15] Dobrica, M. B., Fillon, M., Pascovici, M. D., and Cicone, T., 2010, "Optimizing Surface Texture for Hydrodynamic Lubricated Contacts Using a Mass-Conserving Numerical Approach," Pro. I. Mech. Eng. J-J.Eng. Tribol., **224**(8), pp. 737–750.
[16] Papadopoulos, C. I., Nikolakopoulos, P. G., and Kaiktsis, L., 2011, "Evolutionary Optimization of Micro-Thrust Bearings With Periodic Partial Trapezoidal Surface Texturing," ASME J. Eng. Gas Turb. Power, **133**, pp. 1–10.
[17] Papadopoulos, C. I., Efstathiou, E. E., Nikolakopoulos, P. G., and Kaiktsis, L., 2011, "Geometry Optimization of Textured Three-Dimensional Micro-Thrust Bearings," ASME J. Tribol., **133**(4), pp. 1–14.
[18] Jintanawan, T., Roger Ku, C.-P., and Zhu, J., 2004, "Effects of Thrust Hydrodynamic Bearing Stiffness and Damping on Disk-Spindle Axial Vibration in Hard Disk Drives," Microsystem Tech., **10**(4), pp. 338–344.
[19] Liu, R., Wang, X., 2011, "Dynamic Characteristics Analysis of Micro Air Spiral Grooved Thrust Bearing-Rotor System," Proceedings of the 2011 Institute of Electrical and Electronics Engineers (IEEE) International Conference on Nano/Micro Engineered and Molecular Systems (NEMS), Kaohsiung, Taiwan, February 20–23, pp. 719–723.
[20] Chen, M. F., and Lin, Y. T., 2002, "Static Behavior and Dynamic Stability Analysis of Grooved Rectangular Aerostatic Thrust Bearings by Modified Resistance Network Method," Tribol. Int., **35**(5), pp. 329–338.
[21] Jang, G. H., and Lee, C. I., 2007, "Development of an HDD Spindle Motor With Increased Stiffness and Damping Coefficients by Utilizing a Stationary Permanent Magnet," IEEE Trans. Magn., **43**(6), pp. 2570–2572.
[22] Lee, J., Jang, G., Jung, K., and Ha, H., 2011, "Stability Analysis of a Whirling Disk-Spindle System Supported by FDBs With Rotating Grooves," Microsystem Tech., **17**(5–7), pp. 787–797.
[23] Storteig, E., and White, M. F., 1999, "Dynamic Characteristics of Hydrodynamically Lubricated Fixed-Pad Thrust Bearings," Wear, **232**(2), pp. 250–255.
[24] Zhao, H., Choy, F. K., and Braun, M. J., 2005, "Dynamic Characteristics and Stability Analysis of a Wavy Thrust Bearing," Tribol Trans., **48**(1), pp. 133–139.
[25] Jang, G., and Lee, S., 2006, "Determination of the Dynamic Coefficients of the Coupled Journal and Thrust Bearings by the Perturbation Method," Proceedings of the STLE/ASME 2006 International Joint Tribology Conference, San Antonio, TX, October 23–25, ASME Paper No. IJTC2006-12184, pp. 445–453.